Chinese Journal of Aeronautics, (2019), xxx(xx): xxx–xxx

Chinese Society of Aeronautics and Astronautics
& Beihang University

Chinese Journal of Aeronautics

cja@buaa.edu.cn
www.sciencedirect.com

Experimental validation of a new morphing trailing edge system using Price – Païdoussis wind tunnel tests

D. COMMUNIER, R.M. BOTEZ *, T. WONG

Laboratory of Applied Research in Active Controls, Avionics and AeroServoElasticity (LARCASE), ETS, Montréal H3C 1K3, Canada

Received 19 June 2018; revised 27 July 2018; accepted 24 October 2018

KEYWORDS

Aerodynamic performances;
Aileron;
Morphing wing;
Trailing edge;
Wing tunnel tests

Abstract This paper presents the design and manufacturing of a new morphing wing system carried out at the Laboratory of Applied Research in Active Controls, Avionics and AeroServoElasticity (LARCASE) at the ETS in Montréal. This first version of a morphing wing allows the deformation of its trailing edge, denote by Morphing Trailing Edge (MTE). In order to characterize the technical impact of this deformation, we compare its performance with that of a rigid aileron by testing in the LARCASE's price—Païdoussis subsonic wind tunnel. The first set of results shows that it is possible to replace an aileron by a MTE on a wing, as an improvement was observed for the MTE aerodynamic performances with respect to the aileron aerodynamic performances. The improvement consisted in the fact that the drag coefficient was smaller, and the lift-to-drag ratio was higher for the same lift coefficient.

1. Introduction

Due to its monitoring function, an Unmanned Aerial Vehicle (UAV) makes irregular flights, in which, the flight conditions change frequently and significantly. For a conventional aircraft, the surface of the wing is fixed. That is, airfoils representing wing shapes are chosen and utilized throughout the aircraft's design. As the aircraft passes through different flight phases (climb, descent, and cruise), a compromise is considered to obtain the best efficiency of the global flight. If this efficiency is compared to the optimal efficiency for each flight phase, the efficiency of each phase will be less optimal than the total efficiency. This loss of efficiency would results in higher fuel consumption and/or a shorter operating time.[1–3]

The first objective is to modify the geometrical shape of the wing according to flight conditions with the aim to reach as much as possible its optimal shape for each flight condition. The morphing wing will be designed to increase its aerodynamic performance by increasing lift-drag ratio, which therefore would be equivalent to the increase of the lift and reduction of the drag. This fact will have the effect of reducing fuel consumption, increasing flight autonomy, etc.

* Corresponding author.
E-mail address: ruxandra.botez@etsmtl.ca (R.M. BOTEZ).
Peer review under responsibility of Editorial Committee of CJA.

ELSEVIER Production and hosting by Elsevier

https://doi.org/10.1016/j.cja.2019.03.016

Please cite this article in press as: COMMUNIER D et al. Experimental validation of a new morphing trailing edge system using Price – Païdoussis wind tunnel tests, *Chin J Aeronaut* (2019), https://doi.org/10.1016/j.cja.2019.03.016

Nomenclature

C_L	lift coefficient	y	displacement of the trailing edge
C_D	drag coefficient	p	depth of slit
e	airfoil thickness	l	width of slit
t	thickness of the slit	α	Angle of the morphing trailing edge
L	distance between slit and trailing edge	n	number of slits
y_t	total displacement		

The second objective is to keep the wing weight less than or equal to its current weight. To perform this objective, the structure of the current wing should be analyzed to establish its design criteria (weight, flexural strength and torsion, maximum permissible load), and to further design a new wing that meets these design criteria.

The morphing wings are studied at our Laboratory of Applied Research in Active Controls, Avionics and AeroServoElasticity (LARCASE) at the ETS since 2003. Indeed, this team has already explored numerous development strategies for morphing wing technologies. This research was carried out as part of two major projects of the Consortium of Research and Innovation in Aerospace in Quebec (CRIAQ). CRIAQ projects are carried out within the framework of signed agreements between universities, industrial partners and research institutes. Each of these projects has led to the designing and manufacturing of prototypes and their experimental wind tunnel tests, and to publications of results in scientific journals and conferences. These projects, CRIAQ 7.1 and CRIAQ MDO 505, were carried out in collaboration with Bombardier, Thales, NRC-IAR and École Polytechnique in Canada. In addition, the CRIAQ MDO 505 project was realized in collaboration with Italian partners, Alenia, CIRA, and the University of Naples—Frederico II. These two studies carried out under the leadership of LARCASE team aimed at deforming the upper surface of the morphing wing in order to improve its aerodynamic performance. The first project was called CRIAQ 7.1, in which the deformation of the upper surface was applied to a wing using "Smart Material Actuators" (SMA).[4,5] The resulting deformation made it possible to delay the flow transition on the wing. An ideal rectangular "wing" was used, and therefore no existing structural constraints for a real wing were considered. This concept was experimentally validated in the NRC-IAR wind tunnel. The second CRIAQ project was called the CRIAQ MDO 505 project,[6–8] where MDO stands for "Multidisciplinary Design Optimization". The objective was to design and validate a wing with an aileron. For that wing, it was necessary to move the passage of the air flow along the chord of the wing in order to delay the transition from the laminar to the turbulent flow. In order to perform this motion, the wing tip was equipped with four punctual actuators to change its aileron shape design for a real regional Bombardier aircraft that exhibited structural constraints. The experimental results showed that the system could produce the delay of the airflow transition. A subsequent project with an airfoil of an ATR 42 (Regional Transport Aircraft) made it possible to modify the morphing wing upper surface by means of two oval spars.[9] When those spars rotated, the surface was pushed outwards. This system therefore makes it possible to change the surface outward but not inward, and therefore the improvement of the aerodynamic performances was limited. These deformation methods allowed modification of the airflow, but they proved to be limited in modifying the coefficients values for aerodynamic performance improvement on the morphing ATR-42 wing (less than 5% for the lift and less than 2% for the drag[7]). From these three projects, in order to significantly improve the aerodynamic coefficients of a wing[10] (for example, an increase of more than 50% of the lift with an increase of lift-to-drag ratio L/D), the deformation of the upper surface alone was not sufficient. Therefore, in this work, the design and experimental validation of a morphing wing trailing edge system are analyzed.

Concerning the state of the art in wing morphing, we can refer to the work of Sofla et al.[11]

2. Design of the morphing wing system

2.1. Deformation of the camber

Studies have shown that the most promising type of deformation to meet this study objectives would be the deformation of an airfoil's camber.[12] Indeed, by modifying the camber of an airfoil, it could be possible, for example, to convert a NACA0012 airfoil into a NACA4412 airfoil, thereby attaining a significant increase of the lift of the wing while incurring a smaller increase of the drag, thus resulting in a higher L/D. National Advisory Committee for Aeronautics (NACA) airfoils, whose names consist of two digits and a two-digit number (convention for NACA airfoil with 4 digits), follow the following standard: the first digit denotes the maximum camber of the airfoil as a percentage of the chord; the second digit gives the position of this maximum camber in tens of percent of the chord; the third number (the last two digits) represents the thickness of the airfoil at a percentage of the chord.[13]

Two types of deformations, combined together, made possible to change an airfoil's camber; and these deformations are: the deformation of the leading edge and the deformation of the trailing edge.[14] However, an often encountered problem when the shape of the airfoil deforms consists in the occurrence of waves on the surface of the wing dues to the interactions between the actuating system and the wing structure.[15]

Another difficulty encountered in the development of a morphing wing mechanism for reduced sized aircraft is its weight and its bulk. Any gain in aerodynamic performance (lift, drag) could thus be cancelled out by the additional weight of the mechanism. This is our motivation for developing a mechanism that can improve the aerodynamic performance of a morphing wing without increasing its weight.

Please cite this article in press as: COMMUNIER D et al. Experimental validation of a new morphing trailing edge system using Price – Païdoussis wind tunnel tests, *Chin J Aeronaut* (2019), https://doi.org/10.1016/j.cja.2019.03.016

2.2. Deformation of the trailing edge

A morphing aileron system was developed as part of the CRIAQ MDO 505 project.[16] This system made it possible to operate an articulated aileron from an arm that was rotated, which allowed the shape of the aileron to be changed without the need for a mechanism external to the aileron. Research in Germany at Braunschweig presented a concept of the deformation of the ribs at the trailing edge of the wing using an articulated skeleton.[17] Their report concluded that using the deformation of the trailing edge, it would be possible to replace the ailerons at the end of the wing, but that this deformation alone would not be sufficient to replace the flaps on the wing.

Many research studies have been carried out on the morphing trailing edge, using different actuators types (mechanical, piezoelectric, smart materials actuators). The mechanical deformations were mainly done using articulated ribs like fingers[18,19] using a morphing structure[20,21] (compliant mechanisms). These mechanisms made possible to control the deformation of the structure, but the surface of the wing did not completely respect the desired deformations (wave formations on the surface). In addition, the necessary actuators were often heavy and bulky. The use of smart material actuators[22–24] made it possible to replace mechanical actuators. This reduced the weight of the system but required greater power consumption in return. Another method considered the acting on the surface directly using piezoelectric materials.[25,26] However, these materials only allowed small displacements, and required large electrical consumption.

In our work, to obtain a deformation of the trailing edge rib, vertical incisions were made. Depending on the length, the number and the width of these incisions, it is possible to modify the flexibility of the rib and the amplitude of the deformation. To control the deformation of the rib, a servomotor is used that acts directly on the trailing edge as shown in Fig. 1.

In order to analyze the aerodynamics of the deformed rib, it is firstly necessary to compute its structural deformation using a Finite Element Analysis (FEA) modelling in CATIA V5 as illustrated in Fig. 2.

From the results of the Finite Element Analysis, the contour of the deformed rib was extracted using the PROFSCAN tool.[27] PROFSCAN can draw a curve from an image to create a ".DAT" file that is used further in the XFLR5 software (Fig. 3). To compare the aerodynamic efficiency of the two airfoils, a wing was defined with the same geometrical dimensions as the reference wing previously studied at the LARCASE[28]: 10 in (254 mm) for the chord and 11.5 in (292.1 mm) for the span. This wing was analyzed for the inclined, rigid aileron,

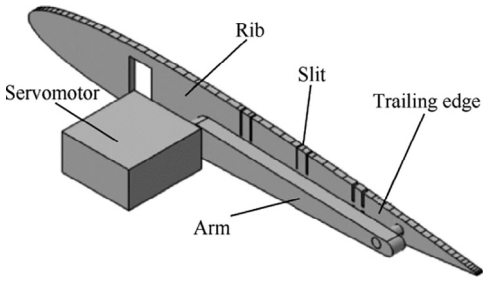

Fig. 1 Control of the trailing edge rib deformation.

Fig. 2 Deformed rib in CATIA V5.

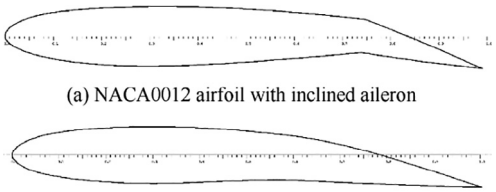

Fig. 3 NACA0012 airfoil with inclined aileron and MTE.

and then, for the Morphing Trailing Edge (MTE), both with a vertical displacement of trailing edge corresponding at 6.8% of the chord.

The curves presented in Fig. 4 compare the performance of a wing with an inclined aileron and that of a wing with a MTE for the airfoils presented in Fig. 3(a), and in Fig. 3(b). The calculations were carried out for a speed of 20 m/s (65.62 ft/s) using the 3D Panels method of the XFLR5 code.[29] The 3D Panels method calculates the aerodynamic flow around a wing quickly. This method alone does not allow to obtain the viscous flow characteristics (parameters), but by using the XFoil analysis on the wing airfoils (2D), an extrapolation was made to calculate the viscous flow for the wing (3D). XFLR5 proposes another method of calculation, but we prefer this method because it allow us to recover the distribution of the coefficients of pressure on the upper and lower surfaces of the wing in order to carry out an aero structural analysis on CATIA V5.[28] The calculation method does not allow for the aerodynamic coefficients to be computed after the stall of the air flow, and for this reason, the calculations stop at the angle of 14°.

Regarding the drag coefficient reduction, the MTE generates less drag than the inclination of the aileron for the same displacement, which meets our goal. This decrease in drag comes mainly from the fact that the deformation of the camber takes place on a larger portion of the wing chord than the deformation of the camber induced by the aileron. The size of the aileron was chosen accordingly to its required geometry by the aircraft model (~25% of the chord), and the length of deformation according to the chord of the MTE was chosen to be close to a NACA4412 airfoil chord, so that a variation of camber from 40% of the chord to the leading edge was obtained.

The wing with an inclined aileron generates more lift than the MTE for their same vertical displacement of the trailing edge of 6.8% of the chord. Wing with inclined aileron generates more lift but they incur more drag, while the MTE generates less drag but also less lift. Therefore, it is difficult to determine which system is the most efficient from the point of view of these two forces. However, the variation of the L/D with the angle of attack is traced in Fig. 4(c) to indicate which system would have the best L/D.

The L/D variation with the angle of attack presented in Fig. 4(c) shows that the MTE has a better L/D than an inclined

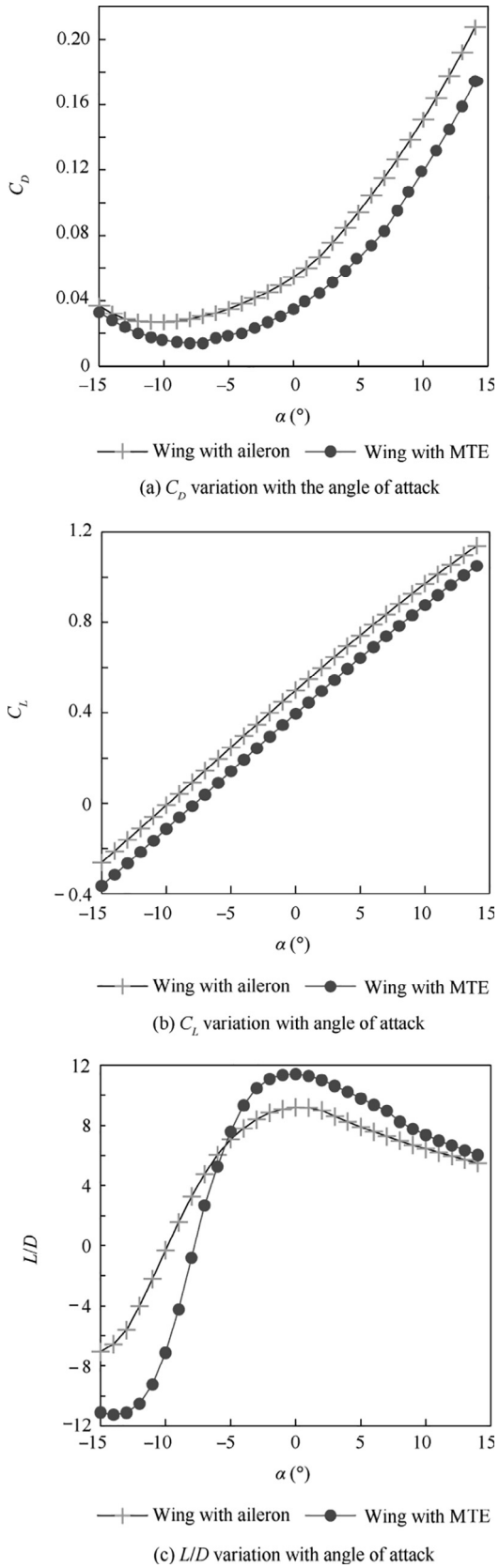

(a) C_D variation with the angle of attack

(b) C_L variation with angle of attack

(c) L/D variation with angle of attack

Fig. 4 Comparation of the performance of a wing with inclined aileron and MTE.

aileron for angles of attack higher than −5°; thus, the MTE is more efficient than the inclined aileron for positive angles of attack. These first theoretical results encouraged us to continue in this direction in order to obtain experimental results.

In the next section, we will discuss on the ways in which the slits in the ribs were sized through design to obtain the MTE that was manufactured using wood.

3. Sizing design and control of the MTE

3.1. Sizing design

To achieve rib flexibility, the anisotropic property of wood was used. Using the fibers in the direction of the chord of the airfoil and making a slit section on the thickness of the airfoil, the bending points were created according to the characteristics of the "compliant mechanisms".[30] These bending points behave like "pivot points"[31] by allowing the simplification of the calculation of the maximum displacement of the MTE. The advantage of this design using bending pivots with respect to a conventional design with mechanical pivots is that there is no need for a mechanism to allow the rotation of the MTE. This fact reduces the weight of the assembly, and facilitates wing maintenance. In order to reduce the force required to bend the rib, the slit (see Fig. 1) must be designed as deep as possible, while keeping enough material for the rib structure to withstand tangential stresses. In order to find out the values of these stresses, the aerodynamic forces were firstly computed on the MTE.

For the first prototype, no sizing calculations were made, and the already acquired experience in wooden wing design and fabrication was sufficient for its manufacturing. In addition, to facilitate the prototype design, the symmetrical slits were dimensioned with symmetrical airfoils that allowed the MTE to change its shape by moving upwards and downwards. The slit was considered as a pivot point, and its displacement for a given width in the rib was calculated. Fig. 5 illustrates the parameters required for the rib deformation calculation.

From Fig. 5, the following equations are obtained as the rib is symmetrical:

$$p = (e - t)/2 \tag{1}$$

$$l = p \times \tan\alpha \tag{2}$$

$$y = L \times \tan\alpha \tag{3}$$

The displacement y depends on the dimensions of the slit according to the next equation:

$$y = (l \times L)/p \tag{4}$$

To obtain this equation, the slits were considered as pivot and so the equation correspond to an angle return.

As we have n slits in the rib, we get the total displacement given by

$$y_t = \sum_{i=1}^{n} y_i \tag{5}$$

$$y_t = \sum_{i=1}^{n} (l_i \times L_i)/p_i \tag{6}$$

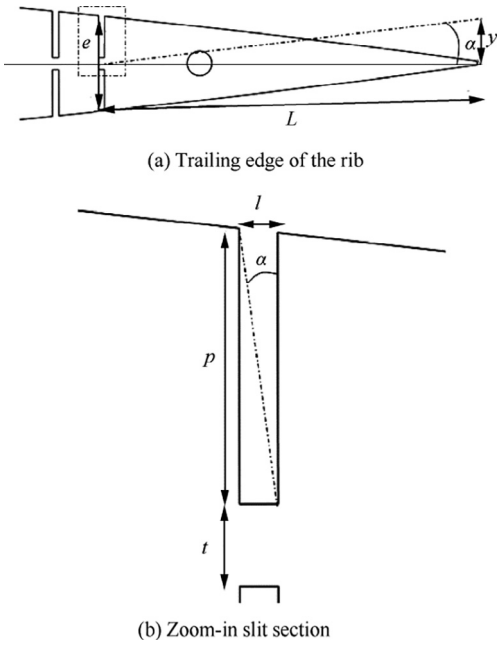

(a) Trailing edge of the rib

(b) Zoom-in slit section

Fig. 5 Deformation of the rib.

3.2. MTE control

The deformation of the MTE is controlled by a servomotor via a rod connected to the trailing edge (see Fig. 1). In order for the system to operate properly, the actuator must deliver sufficient torque. A FEA was performed to obtain the needed torque for the control of the wing under aerodynamical pressures (20 m/s = 65.62 ft/s) with an angle of attack of 15°, as shown on Fig. 6, the surface stresses caused by the aerodynamic pressure were low. The servomotor must mainly counter the elastic resistance of the ribs. The geometry of the ribs makes their resistance to be very low. However, the servomotor provides enough forces to counteract the aerodynamic forces on these ribs. For the prototype, the same servomotor as the one for a conventional aileron was used (Fig. 7). Therefore, the morphing mechanism was transferred on a conventional wing without changing its weight from the point of view of the controls.

In the next section, the manufacturing of the MTE system and, the results of the wind tunnel test are presented.

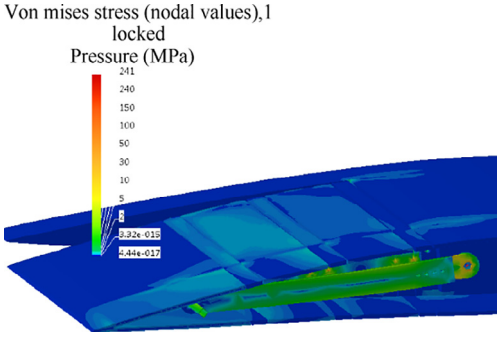

Fig. 6 FEA of MTE control under aerodynamical pressures.

ANNOUNCED SPECIFICATION OF HS-5645MG STANDARD SPORT DIGITAL HIGH TORQUE SERVO

1.TECHNICAL VALUES		
CONTROL SYSTEM	:+PULSE WIDTH CONTROL 1500usec NEUTRAL	
OPERATING VOLTAGE RANGE	:4.8V TO 6.0V	
OPERATING TEMPERATURE RANGE	:-20 TO +60°C	
TEST VOLTAGE	:AT 4.8V	:AT 6.0V
OPERATING SPEED	:0.23sec/60° AT NO LOAD	:0.18sec/60° AT NO LOAD
STALL TORQUE	:10.3kg.cm(143.03oz.in)	:12.1kg.cm(168.03oz.in)
OPERATING ANGLE	:45°ONE SIDE PULSE TRAVELING 400usec	
DIRECTION	:CLOCK WISE/PULSE TRAVELING 1500 TO 1900usec	
IDLE CURRENT	:3mA	:3mA
RUNNING CURRENT	:350mA	:450mA
DEAD BAND WIDTH	:1usec	
CONNECTOR WIRE LENGTH	:300mm(11.81in)	
DIMENSIONS	:40.6x19.8x37.8mm(1.59x0.77x1.48in)	
WEIGHT	:60g(2.11oz)	

Fig. 7 Servomotor specifications.

4. Manufacturing and wind tunnel testing

4.1. Manufacturing of the MTE system

LASER cutting machine was used to manufacture both test wings, and allowed obtaining their components quickly and at a reasonable cost. To validate the functionality of this MTE, a prototype was manufactured to deform three ribs as shown in Fig. 8. Fig. 9 shows the system including the ribs deformation. The trailing edge is shown on the right hand side of Figs. 8 and 9. The structure of the wing is simple as is equipped with a main spar and three ribs. The thin spars have a main purpose of helping during the manufacturing process but are not required in the wing structure because balsa sheeting is added to cover the wing and the main spar is designed to support all the loads on the wing.

4.2. Wind tunnel tests

The numerical results were validated by means of wind tunnel tests on the various morphing wings. The morphing wings have the same dimensions as the reference wing (Fig. 10(a)), so that the impact of the system on the morphing wing was compared to the same wing without any deformation system (the reference wing). The reference wing has the NACA0012 airfoil with a chord of 10 in (254 mm) and a wingspan of 11.5 in (292.1 mm). The 10 in (254 mm) chord relates to the chord of the test wing of the ATR42 research project at the LARCASE which also was of 10 in (254 mm). The wing span is 12 in (304.8 mm), which corresponds to the mid-height of the wind tunnel test chamber, but 0.5 in (12.7 mm) is embedded in the base of the wing that is attached to the aerodynamic scale, which is the reason why the analysis is carried out on a wing with a span of 11.5 in (292.1 mm). The aerodynamic scales is used to measure the loads (forces and moments) on the aerodynamic model installed in the wind tunnel.

An objective of the design of the reference wing was to validate firstly the functioning of the LARCASE aerodynamic

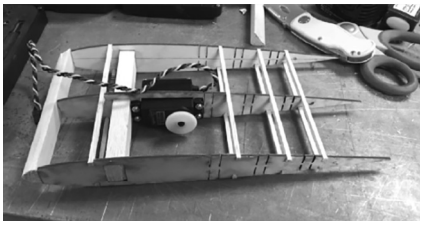

Fig. 8 Structure of the MTE system.

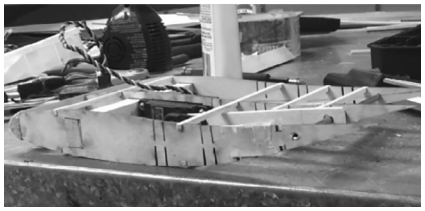

Fig. 9 Prototype with a MTE system.

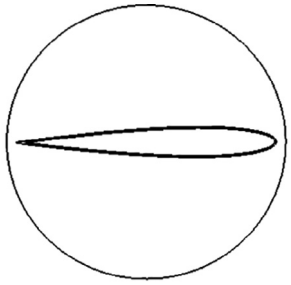

(a) Top view of the reference rigid wing

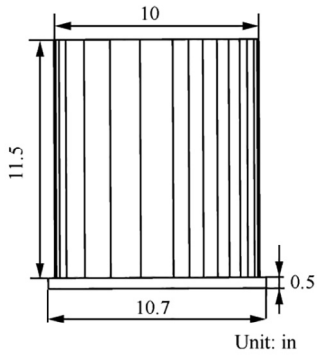

(b) Side view of the reference rigid wing

Fig. 10 Reference rigid wing dimensions.

scales by comparing the measured values with the numerical values of the loads (forces and moments) acting on the wing. Fig. 10(b) shows the dimensions of the reference wing.

Wind tunnel tests were performed on this reference wing as part of the Master's thesis of the main author,[32] in which the experimental aerodynamic performances with respect to their numerical values computed by XFLR5 software[28] were compared, and further validated. The tests were carried out in the Price-Païdoussis wind tunnel's rectangular test chamber (2 ft (609.6 mm) × 3 ft (914.4 mm), Fig. 11) at speeds of 20 m/s (65.62 ft/s), 25 m/s (82.02 ft/s), 30 m/s (98.43 ft/s) and 35 m/s (114.83 ft/s). The Price-Païdoussis wind tunnel can reach a maximum speed of 37 m/s (121.39 ft/s) for this test chamber.

Fig. 11 LARCASE Price-Païdoussis subsonic wind tunnel.

The angle of attack of the wing was changed from −10° to 20° by 1° steps. The measurements were carried out with an aerodynamic scales equipped with an Omega 160 force sensor from ATI Industrial Automation. Its technical details expressed in term of maximum loads (forces and moments) are presented in Table 1. This scale was designed by the LARCASE team. Following the manufacturer's specifications, it was possible to improve the resolution of the sensor, as well as its accuracy by filtering the measurement given by the aerodynamic scales. This filtering allowed us to obtain resolution of 0.01 N with a maximum error of 0.1 N due to the rotation mechanism of the aerodynamic scales. The applied digital filtering enable higher accuracy sampling of the drag force. The theoretical values of the lift, the drag and the pitch coefficients were calculated with the "3D Panels" method by using XFLR5 code for a wing with the span of 11.5 in (254 mm) and the chord of 10 in (292.1 mm). The wing in the wind tunnel was in contact with the floor of the test chamber, and this contact was simulated using the symmetry of the span in the XFLR5 code. The calculated wing therefore had a total span of 23 in (584.2 mm). Figs. 12–14 show the variation of the drag, lift and pitch coefficients of the wing with the angles of attack. The measured values in the wind tunnel are compared to the calculated values using XFLR5 code.

At a speed of 20 m/s (65.62 ft/s), the wing has a stall angle of 18°, and at a speed of 25 m/s (82.02 ft/s), the stall occurs at 19°. For a speed of 30 m/s (98.43 ft/s) and 35 m/s (114.83 ft/s), there was no stall occurrence before 20°. The stall angles at 20 m/s (65.62 ft/s) and 25 m/s (82.02 ft/s) were not obtained during the calculations because of the fact that the calculation method does not allow the coefficients to be computed.[28]

The objective of the static test is to validate that the mechanism of the MTE is morphed when a command is sent to the system. There is the need to validate that this experimental deformation of the MTE corresponds to the calculated deformation. For the static tests, a command was sent to the servomotor controlling the MTE, and the vertical displacement at the tip of the trailing edge was measured.

Fig. 15 shows the dimensioned slits necessary to calculate the total deformation of a rib of the wing. An optimization method was not used to determine the number of slots and their dimensions. Instead, an iterative method using FEA module of CATIA V5 was used, by manually changing the sizes of the slits according to the stresses on the ribs obtained using FEA. The main objective of static tests was to obtain the deformation of the inclined aileron presented in Fig. 15 with the constraints, expressed in term of the torque available by the actuator and the mechanical strength of the wood used for the prototype (plywood[33]).

The Table 2 lists the dimensions of the slits from left to right in inches.

According to Eq. (6) and values of l_n, L_n and p_n given in Table 2, the maximum displacement y_t is calculated as

Table 1 Range and resolution for ATI Omega 160 F/T sensor.

Technical index	F_x, F_y	F_z	T_x, T_y	T_z
Sensing range	2500 N (600 lbf)	6250 N (1500 lbf)	400 N·m (3600 lbf·in)	400 N·m (3600 lbf·in)
Resolution	1/2N (1/8 lbf)	3/4 N (1/4 lbf)	1/20 N·m (1/2 lbf·in)	1/20 N·m (1/4 lbf·in)

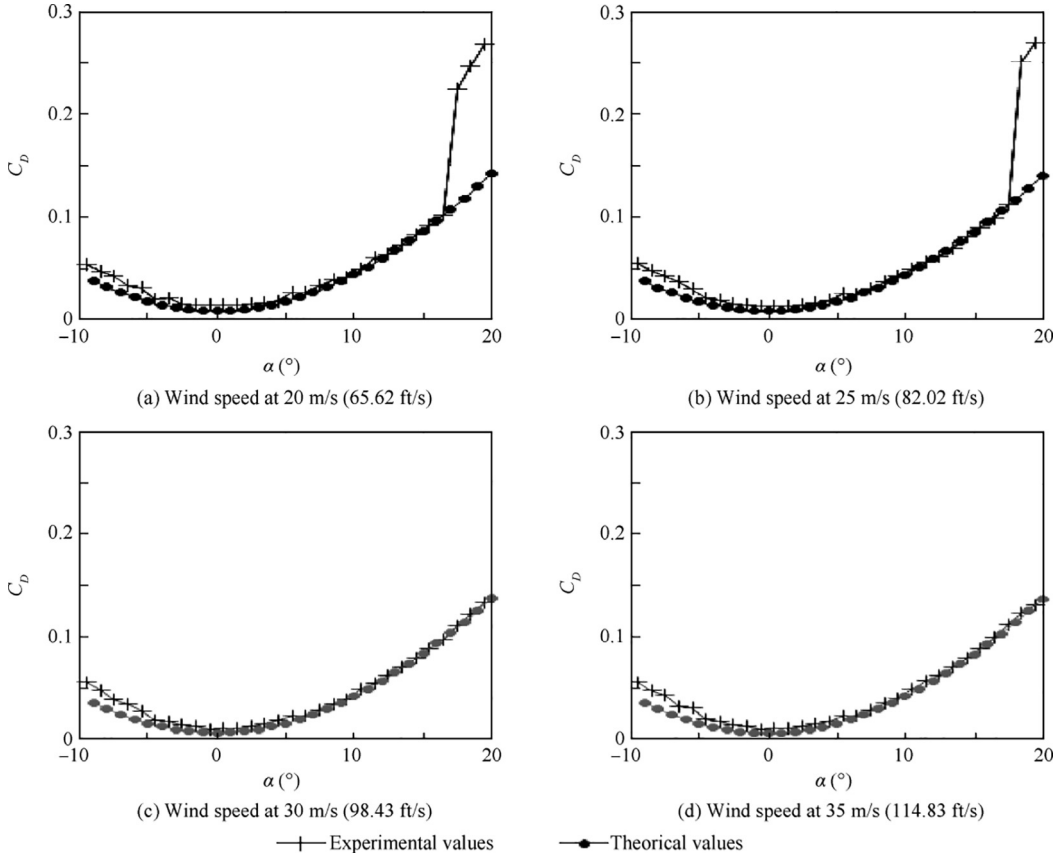

Fig. 12 Drag coefficients variation with angle of attack for the reference wing.

$$y_t = \frac{0.026 \times 4.911}{0.416} + \frac{0.026 \times 4.635}{0.4} + \frac{0.021 \times 3.609}{0.34} + \frac{0.021 \times 3.338}{0.317} + \frac{0.014 \times 2.317}{0.233} + \frac{0.014 \times 2.053}{0.205} = 1.33 \text{ in} \quad (7)$$

Fig. 16 illustrates the measurement of the displacement of the trailing edge during a 7° rotation of the actuator.

The distance between the axis of the servomotor that controls the deformation and the axis that moves the trailing edge is 4.25 in (107.95 mm) and the distance between the axis of the servomotor and the trailing edge is 5.6 in (142.24 mm) (Fig. 17). Thus, for a displacement of the servomotor axis of 7°, the displacement of the trailing edge axis is 0.52 in (13.21 mm) according to the Eq. (3). For a linear displacement of the trailing edge, this displacement would be 0.69 in (17.526 mm). Since the deformation is given by six articulations (joints) that are not aligned on the actuator axis, the MTE does not move along the same axis as the actuator arm. These calculations do not give a precise value for the displacement; a FEA method makes it possible to obtain a very good precision on the deformation value.

Wind Tunnel Tests measurements were performed to validate the dynamic operation of the system. The main objective of these measurements was to validate that the deformation was well carried out in the presence of aerodynamic loads. These tests allowed us to observe the influence of the mechanism on the drag of the wing compared to the drag of the reference wing (without any mechanism). In this section, the MTE is not moved (displaced) by the controller. Wind tunnel measurements with controlled displacement of the MTE will be presented in the next section. Fig. 18 presents the test wing used to obtain the following results, shown in Fig. 19.

Two causes were identified for the increase in drag on the morphing wing with respect to the drag for the reference wing:

(1) The discontinuity between the fixed section of the wing and the moving section of the wing

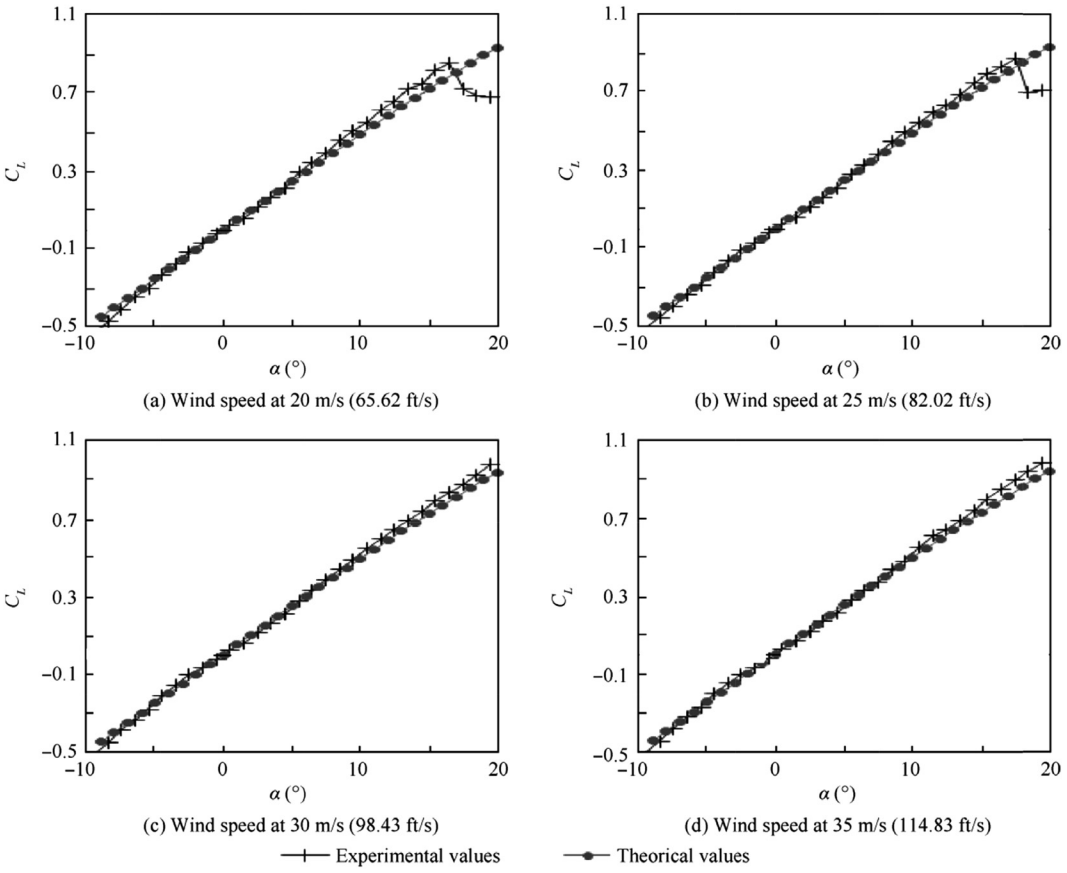

Fig. 13 Lift coefficients variation with angle of attack for the reference wing.

(2) The presence of the slits on the surface of the wing allowing deformations.

The first cause is common to both the aileron and the MTE system. The second cause is due only to the specific design of the MTE system. For this reason, it was chosen to work on the second cause in order to improve the design of the MTE system.

Four experiments were therefore defined to improve the airflow around the wing. The first experiment reproduced a rigid wing by covering all the slits on the wing with tapes (Fig. 20). For the second experiment, the tape covering the intersection between the morphing part and the fixed part of the wing was removed (Fig. 21). For the third experiment, the tapes were installed on one side of the slits (leading edge side) with the aim to hide them but without hampering the deformation (Fig. 22). For the fourth and last experiment (Fig. 23), tapes were installed on both sides of the slits that allowed some deformation of the trailing edge (a bump or a hollow were formed on the tape during the deformation).

The first experiment was conducted to confirm that the drag difference was not due to an imperfection on the wing. The second experiment was performed to identify the influences of the discontinuities between the fixed part and the morphing part of the wing. Experiments 3 and 4 were conducted on improved design of the morphing test wing and had the aim of improving its aerodynamic performances. The drag coefficient measurements obtained with experiments 1–4 were traced versus the drag coefficients obtained numerically for the morphing and reference test wings (Fig. 24).

During Experiment 1, difference was recorded in the stall angles (from 9° to 16° for positive angles and from −16° to −20° for negative angles). Further studies are necessary to identify the cause of this difference. A drag coefficient curve variation similar to that of the reference drag coefficients was observed (Fig. 25).

Experiment 2 indicates that the discontinuity would have a higher influence for an angle of attack close to 0° than the influence for higher angles of attack (±5°). The comparison between results obtained for Experiments 3 and 4 is not obvious. Thus Experiment 3 was found to be more efficient than Experiment 4 for positive angles but less efficient for negative angles (Experiment 3 shows an asymmetry in the results). However, an analysis of the L/D variation with the angle of attack makes it possible to determine that one experiment is more effective than another (Fig. 26). In Fig. 26, the L/D variation with the angle of attack between 4° and 8° for the reference wing is due to the maximum error of 0.1 N on the measurement of the drag force.

5. Comparison of aerodynamics coefficients for a MTE versus a conventional aileron

Studies[17] revealed that elastic trailing edge could be used for adaptive wing. To validate in this paper that the MTE is

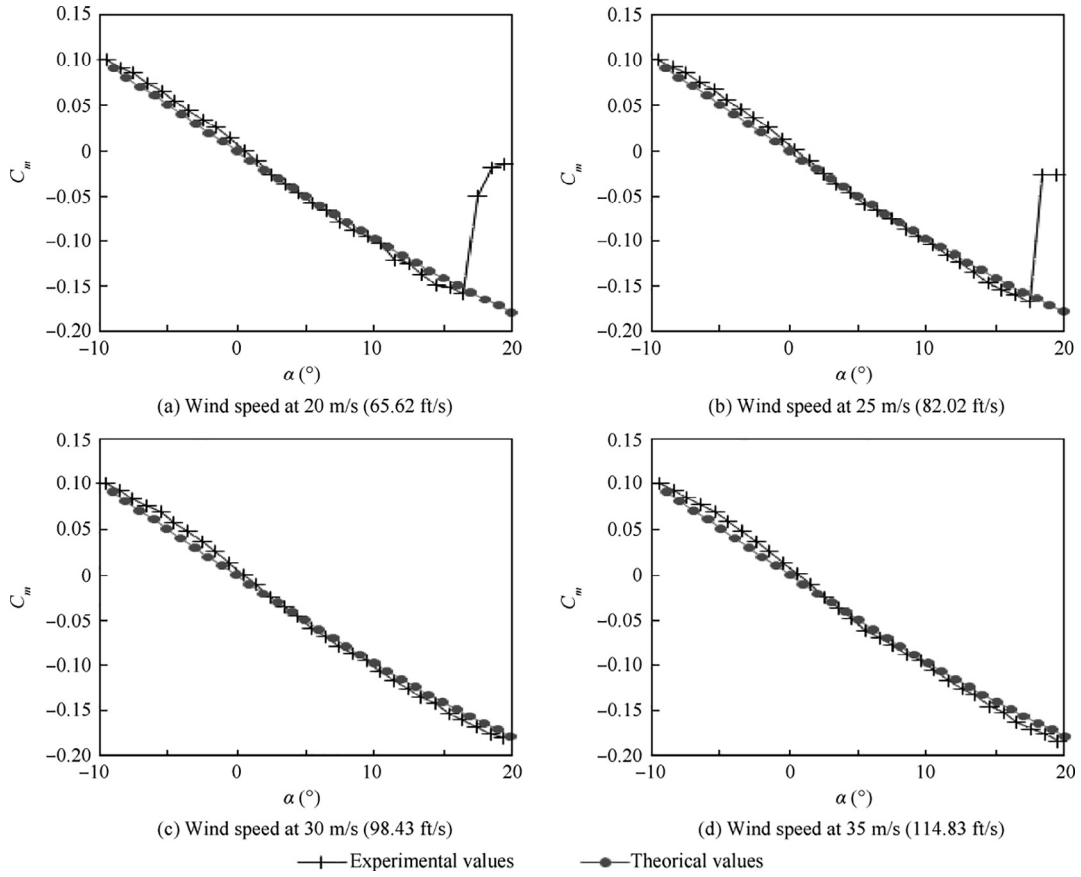

Fig. 14 Pitch coefficients variation with angle of attack for the reference wing.

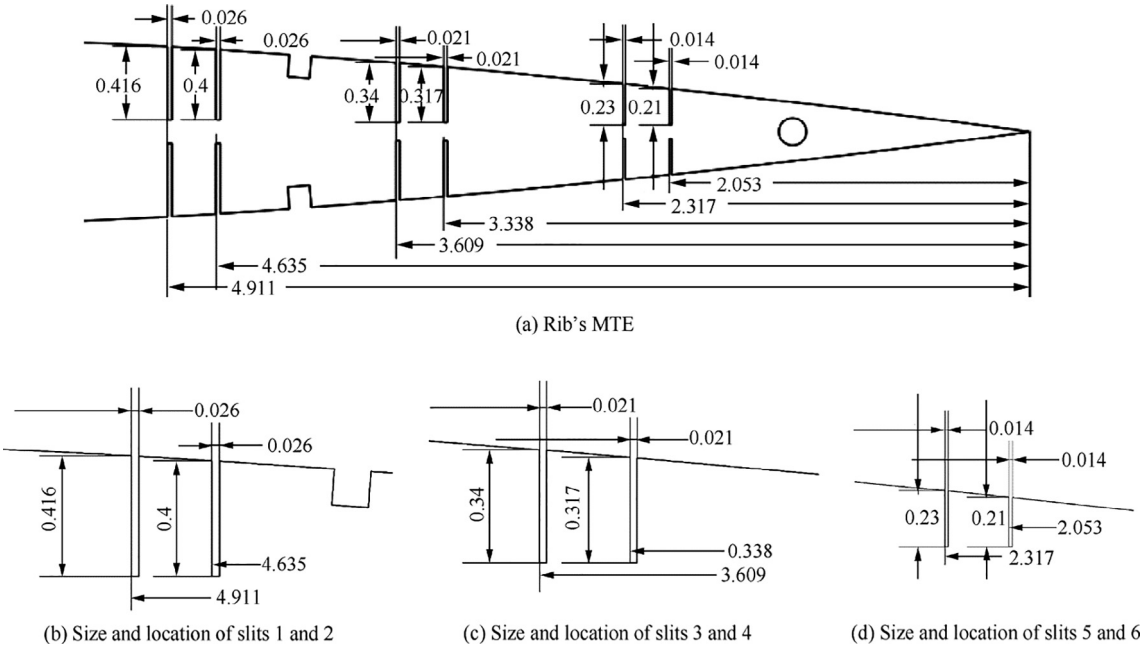

Fig. 15 Size and location of the slits in the MTE rib (unit: in).

Table 2 Size of the slits in the deformable rib.

Slit number	l_n	L_n	p_n
1	0.026	4.911	0.416
2	0.026	4.635	0.4
3	0.021	3.609	0.34
4	0.021	3.338	0.317
5	0.014	2.317	0.233
6	0.014	2.053	0.205

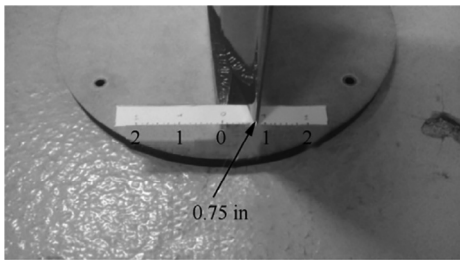

Fig. 16 0.75 in displacement of the trailing edge tip (19.05 mm) for a 7° rotation.

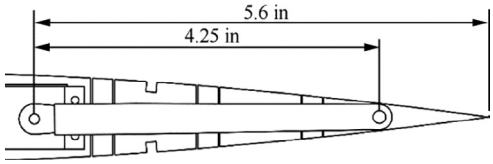

Fig. 17 Controlling distance.

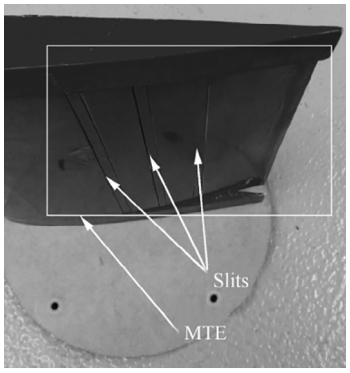

Fig. 18 Test wing with MTE.

capable of replacing an aileron, wind tunnel tests were performed on both, the MTE and also on an aileron.

To perform these wind tunnel tests, a wing was designed and manufactured with its basic dimensions given in Fig. 27, on which we placed an aileron. The width of the aileron is 25% of the wing chord and its span is 9.5 in (241.3 mm). There is 1 in (25.4 mm) on each side of the aileron as shown in Fig. 27.

To be able to retrieve data efficiently, a control interface was added for the aileron to the Labview interface of the aerodynamic balance. Labview software makes it possible to

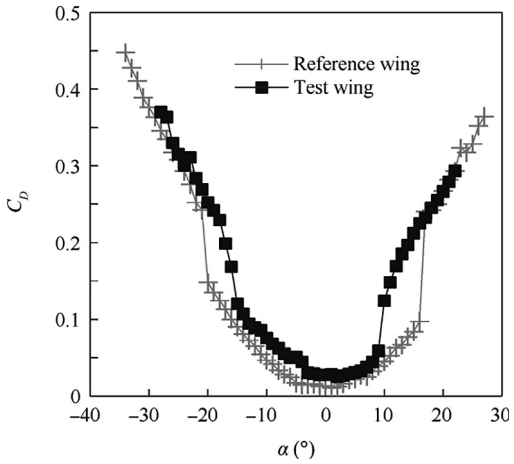

Fig. 19 Influence of the MTE on the drag coefficient at 15 m/s (49.21 ft/s).

Fig. 20 Experiment 1 with all slits covered by tapes (continuous surface).

Fig. 21 Experiment 2 tapes covering the intersection between the morphing fixed parts were removed.

Fig. 22 Experiment 3 with tapes installed on one side of the slits (deflector).

Fig. 23 Experiment 4 with tapes installed on both sides of the slits.

program commands for actuator controls, and to read instrument outputs through a graphical interface that displays results. This interface controls a servomotor by indicating an angle for its control arm. The force was calculated and displayed for each angle of the actuator. To obtain an angle of the servomotor, the forces reading were averaged, and were further saved in a table. As long as this position was kept constant by the servomotor, its average value in the array was updated; when the angle changed, it was the average value of this new angle that was updated. By reviewing all the possible angles, the graph of the forces was drawn as a function of the angle of the servomotor, and the results were directly visualized. A backup function was added to write the values table of to a text file as a means to save the data. Then these values were studied in order to analyze the wings' aerodynamic performance.

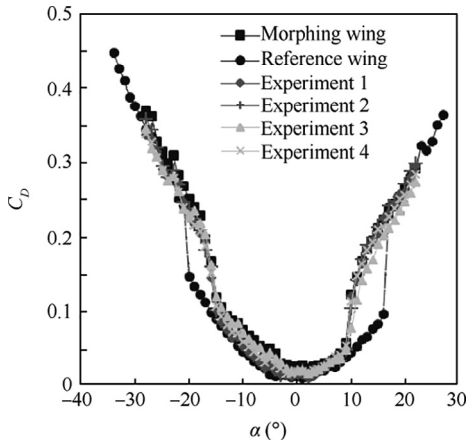

Fig. 24 C_D variation with the angles of attack at the speed of 15 m/s (49.21 ft/s).

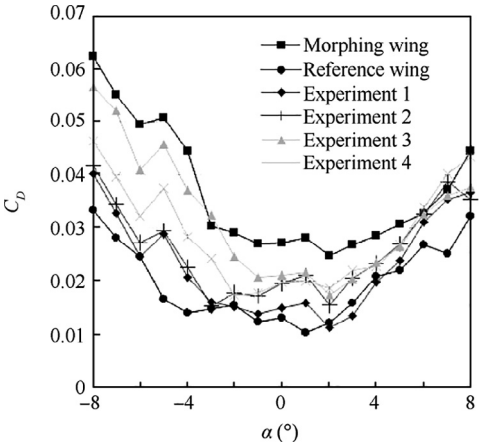

Fig. 25 Zoom-in of the drag coefficients variation with the angles of attack between −8° and 8°.

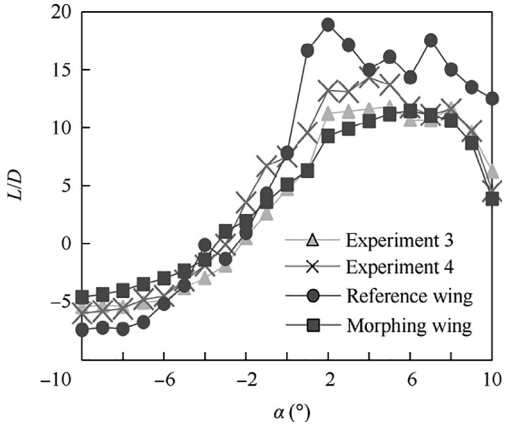

Fig. 26 Wing L/D variation with the angle of attack.

5.1. Comparison of aerodynamics coefficients

In order to determine if the MTE system can replace an aileron on a wing, the corresponding lift and drag coefficients of the

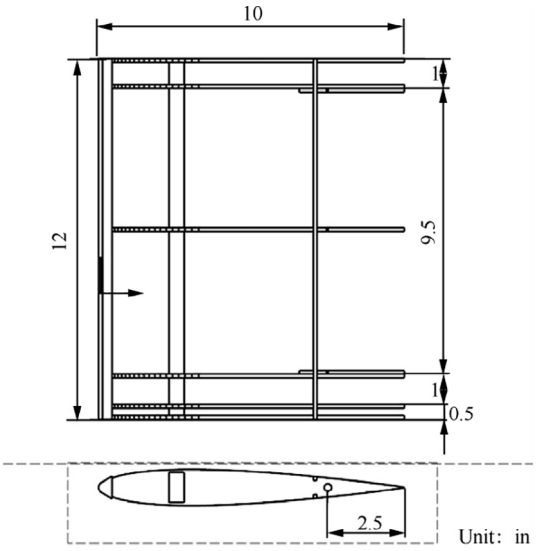

Fig. 27 2D plan of the wing with an aileron.

two systems were compared. Since the angles of the two systems are different, their behaviors are also different; their respective motions cannot be directly compared because of the difference in size between moving surfaces (Fig. 15) and the control arms (Figs. 16 and 17). However, a similar evolution of the lift coefficient was observed for the two systems. As the goal of this paper is to determine if one system creates more drag than another system, the drag of both systems was compared for the same generated lift. The following graphs (Figs. 28 and 29) show the variation of the lift and drag coefficients C_L and C_D with the angle of attack for the aileron and the MTE compared to the C_L and C_D of the reference wing. From these figures, it was observed that the aileron can create a C_L greater than the C_L of the MTE, but the C_D of the aileron was also larger than the C_D of the MTE. Analysis of the behavior of the C_L allowed to define the roll that it could induce, and thus, to determine if the MTE can indeed replace ailerons.[34] This observation alone made it possible to define if one system was more efficient than another.

It was observed that the wing with the MTE created less drag (Fig. 30), and therefore it had a higher L/D (Fig. 31) than the wing with an aileron. It can be therefore concluded that the MTE was more efficient than the aileron for angles of attack between −10° and 10°. Therefore, by replacing the conventional aileron with the MTE should result in a reduction in fuel consumption and further in an increase in aircraft autonomy and efficiency. This observation might also be valid for other aircraft control surfaces such as elevator and rudder.

5.2. Electrical consumption

As the MTE requires deformation of the ribs actuated by the servomotor, the MTE requires more electrical energy to operate than an aileron. For a conventional aileron, without external aerodynamic forces, the servomotor does not need to act to keep the aileron in a fixed position (the wing is placed vertically) but for the MTE, the electrical resistance of the ribs induces an increase of the current required by the servomotor when its deformation is increased. In order to ascertain the

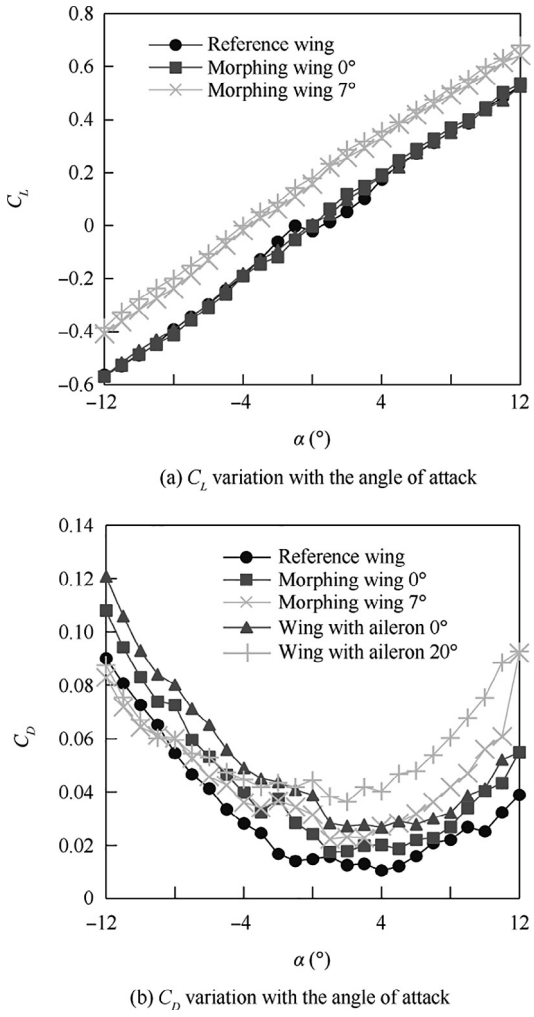

Fig. 28 $C_L$and C_D variation with the angle of attack. At 15 m/s (49.21 ft/s) for each system.

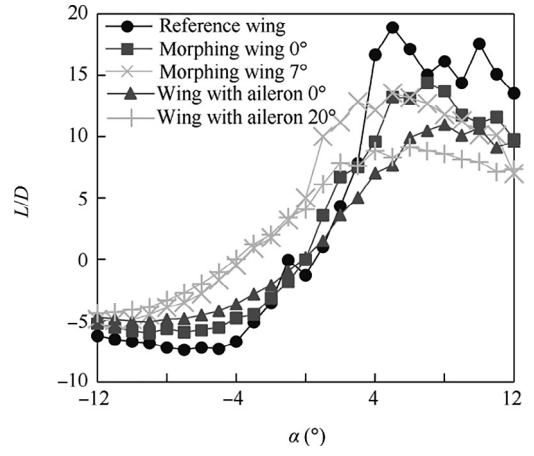

Fig. 29 L/D variation with the angle of attack at 15 m/s (49.21 ft/s) for each system.

magnitude of this difference, the current consumed by the servomotors of the test wings was measured. For the wing equipped with an aileron, the current consumption remains

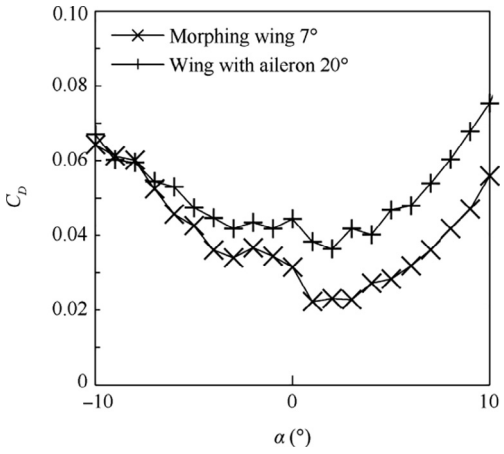

Fig. 30 C_D variation with angle of attack zoomed-in around 0°.

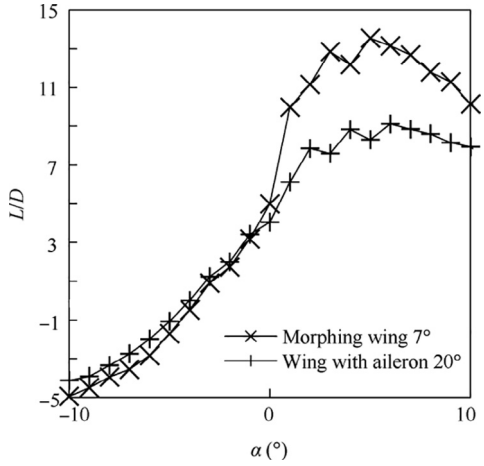

Fig. 31 L/D variation with angle of attack zoomed-in around 0°.

constant at 3.5 mA from −40° to 40°. For the wing with the MTE, the current consumption varies from 3.5 mA at 0° to 70 mA at ± 7° (with a jump from 16 mA at 6° to 70 mA at 7°). The current jump is due to the mechanical limit of the MTE. It is therefore important to accurately measure the travel limits of the MTE to avoid over-consumption of the system that could lead to a breakage of the servomotor. On the other hand, for the two test wings, an increase of the current consumption has not been noticed when an external aerodynamic force was applied. The dimensions of our test wings and the speeds used were too small for the forces, on the control surfaces, to disturb significantly the servomotors.

6. Conclusions

This paper describes the first phase of a new morphing wing project at the LARCASE. The MTE was firstly studied in this paper because this section of the wing was easier to deform (morph) than its other sections. The next step will be to adapt existing MTE design to modify also the leading edge of the wing. That leading edge section is more complicated than the trailing edge section to deform because of its smaller width (20% width for the leading edge and 50% width for the trailing edge), and thus, it is not evident that the morphing leading edge design will achieve a reduction in the wing drag.

However, the results obtained in this paper have shown an improvement in the effectiveness of the MTE on the wing drag, in particular in the sections where the ailerons are located. This comparative study between the MTE and the rigid aileron has verified that the MTE had the same behavior as an aileron regarding the increase of lift with the angle of attack. The drag analysis showed us that the MTE generated less drag than the aileron. Finally, analysis of the L/D has shown that the MTE gave a lower drag for the same lift as an aileron, which led to less fuel consumption. Moreover, the MTE has the same components (rib and actuator) as an aileron, and thus does not increase the weight of the wing (both test wings weight is a total of 725 g (1.6 lb). The use of the MTE led to the satisfaction of the following three criteria: to replace ailerons, to reduce fuel consumption and to maintain the mass of the wing.

Acknowledgments

The authors would like to thank Mr Aurélien Mons for his help in the preliminary design of the MTE, Mr Antoine Machetto for his help in the design of the rotation system of the aerodynamic balance and Mr Théo André for his help in carrying out tests in the wind tunnel for the wing with an aileron. In addition, the authors would like to thank very much to the NSERC for the Canada Research Chair in Aircraft Modeling and Simulation New Technologies Funding.

References

1. Nemec M, Zingg DW, Pulliam TH. Multipoint and multi-objective aerodynamic shape optimization. *AIAA J* 2004;42(6):1057–65.
2. Park K, Han JJ, Kim BS, Lee J. Optimal design of airfoil with high aspect ratio in unmanned aerial vehicles. *World Academy of Science, Engineering and Technology* 2008;2(4):171–77.
3. Barbarino S, Bilgen O, Ajaj RM, Friswell MI, Inman DJ. A review of morphing aircraft. *Journal of Intelligent Material Systems and Structures* 2011;22(9):823–77.
4. Popov AV, Grigorie LT, Botez RM, Mamou M, Mebarki Y. Closed-loop control validation of a morphing wing using wind tunnel tests. *Journal of Aircraft* 2010;47(4):1309–17.
5. Kammegne MJT, Grigorie LT, Botez RM, Koreanschi A. Design and wind tunnel experimental validation of a controlled new rotary actuation system for a morphing wing application. *Proceedings of the Institution of Mechanical Engineers, Part G: Journal of Aerospace* 2016;230(1):132–45.
6. Koreanschi A, Gabor OŞ, Ayrault T, Botez RM, Mamou M, Mebarki Y. Numerical optimization and experimental testing of a morphing wing with aileron system. *24th AIAA/AHS adaptive structures conference*. 2016. p. 1083.
7. Koreanschi A, Sugar-Gabor O, Botez RM. Drag optimisation of a wing equipped with a morphing upper surface. *The Aeronautical Journal* 2016;120(1225):473–93.
8. Michaud F, Joncas S, Botez RM. Design, manufacturing and testing of a small-scale composite morphing wing. *19th confrence on composite materials*. 2013.
9. Gabor OS, Koreanschi A, Botez RM. Low-speed aerodynamic characteristics improvement of ATR 42 airfoil using a morphing wing approach. *IECON 2012-38th annual conference on IEEE Industrial Electronics Society*. 2012.
10. Reich G, Sanders B. Introduction to morphing aircraft research. *Journal of Aircraft* 2007;44(4):1059.

11. Sofla AYN, Meguid SA, Tan KT, Yeo WK. Shape morphing of aircraft wing: Status and challenges. *Materials & Design* 2010;31 (3):1284–92.
12. Sanders B, Eastep FE, Forster E. Aerodynamic and aeroelastic characteristics of wings with conformal control surfaces for morphing aircraft. *Journal of Aircraft* 2003;40(1):94–9.
13. Jacobs EN, Ward KE, Pinkerton RM. The characteristics of 78 related airfoil sections from tests in the variable-density wind tunnel. Washington, D.C.: National Advisory Committee for Aeronautics; 1933. Report No.: 460.
14. Gandhi F, Anusonti-Inthra P. Skin design studies for variable camber morphing airfoils. *Smart Materials and Structures* 2008;17 (1):015025.
15. Peel LD, Mejia J, Narvaez B, Thompson K, Lingala M. Development of a simple morphing wing using elastomeric composites as skins and actuators. *Journal of Mechanical Design* 2009;131(9):091003.
16. Amendola G, Dimino I, Pecora R, Amoroso F, Actuation system design for a morphing aileron. *Applied Mechanics and Materials* 2015;798:582–88.
17. Monner HP, Sachau D, Breitbach E. Design aspects of the elastic trailing edge for an adaptive wing. German Aerospace Center Braunschweig (Germany) Inst of Structural Mechanics; 2000. Report No: ADP010488.
18. Monner HP, Hanselka H, Breitbach EJ. Development and design of flexible fowler flaps for an adaptive wing. *Smart Structures and Materials 1998: Industrial and Commercial Applications of Smart Structures Technologies* 1998;3326:60–71.
19. Poonsong P. Design and analysis of a multi-section variable camber wing [dissertation]. College Park: University of Maryland; 2004.
20. Kota S, Hetrick JA, Osborn R, Paul D, Pendleton E, Flick P, et al. Design and application of compliant mechanisms for morphing aircraft structures. *Smart Structures and Materials 2003: Industrial and Commercial Applications of Smart Structures Technologies* 2003;5054:24–34.
21. Liu SL, Ge WJ, Li SJ. Optimal design of compliant trailing edge for shape changing. *Chinese Journal of Aeronautics* 2008;21 (2):187–92.
22. Elzey DM, Sofla AYN, Wadley HN. A bio-inspired high-authority actuator for shape morphing structures. *Smart structures and materials 2003: Active Materials: Behavior and Mechanics* 2003;5053:92–101.
23. Elzey DM, Sofla AY, Wadley HN. A shape memory-based multifunctional structural actuator panel. *International Journal of solids and Structures* 2005;42(7):1943-55.
24. Berton B. Shape memory alloys application: trailing edge shape control. Dassault Aviation, Saint-Cloud (France); 2006. Report No: ADA479896.
25. Moosavian A, Chae EJ, Pankonien AM, Lee AJ, Inman DJ. A parametric study on a bio-inspired continuously morphing trailing edge. *Bioinspiration, Biomimetics, and Bioreplication* 2017;10162:204.
26. Wang DP, Bartley-Cho JD, Martin CA, Hallam BJ. Development of high-rate large-deflection hingeless trailing-edge control surface for the Smart Wing wind tunnel model. *Smart structures and materials 2001: Industrial and commercial applications of smart structures technologies* 2001;4332:407–19.
27. Aero@Net, Cnc@Net. Utilitaire profscan [Internet]. 2004 Dec [Accessed 13 December 2017]; Available from: http://www.teaser.fr/~abrea/cncnet/logiciel/profscan.phtml.
28. Communier D, Flores Salinas M, Carranza Moyao O, Botez RM. Aero structural modeling of a wing using CATIA V5 and XFLR5 software and experimental validation using the Price-Païdoussis wing tunnel. *AIAA atmospheric flight mechanics conference*. Reston: AIAA; 2015.
29. Onen AS, Cevher L, Senipek M, Mutlu T, Gungor O, Uzunlar IO, et al. Modeling and controller design of a VTOL UAV. *Unmanned Aircraft Systems (ICUAS) 2015 International Conference*; 2015.
30. Howel LL. *Compliant mechanisms*. New York: John Wiley & Sons; 2001.
31. Howle LL, Midha A. A method for the design of compliant mechanisms with small-length flexural pivots. *Journal of Mechanical Design* 1994;116(1):280–90.
32. Communier D. Méthodologie de modélisation aérostructurelle d'une aile utilisant un logiciel de calcul aérodynamique et un logiciel de calcul par éléments finis [dissertation]. Montreal: École de Technologie Supérieure; 2015.
33. Cai Z, Ross RJ. Mechanical properties of wood-based composite materials. *Wood handbook, wood as an engineering material*. 2010. p. 12.
34. Vorobiev AN, Rennie RM, Jumper EJ, McLaughlin TE. Experimental investigation of lift enhancement and roll control using plasma actuators. *Journal of Aircraft* 2008; 45(4):1315-21.